Clin Neuroradiol (2019) 29:75–86
https://doi.org/10.1007/s00062-017-0623-7

ORIGINAL ARTICLE

Characterization of Skull Base Lesions Using Pseudo-Continuous Arterial Spin Labeling

B. Geerts[1,2] · D. Leclercq[1] · S. Tezenas du Montcel[3,4] · B. Law-ye[1,5] · S. Gerber[1] · D. Bernardeschi[6] · D. Galanaud[1,5] · D. Dormont[1,5] · N. Pyatigorskaya[1,5]

Received: 25 May 2017 / Accepted: 19 August 2017 / Published online: 11 September 2017

Abstract

Purpose Pseudo-continuous arterial spin labeling (pCASL) is a non-invasive magnetic resonance (MR) perfusion technique. Our study aimed at estimating the diagnostic performance of the pCASL sequence in assessing the perfusion of skull base lesions both qualitatively and quantitatively and at providing cut-off values for differentiation of specific skull base lesions.

Methods In this study 99 patients with histopathologically confirmed skull base lesions were retrospectively enrolled. Based on a pathological analysis, the lesions were classified as hypervascular and non-hypervascular. Patients were divided into two subgroups according to the anatomical origin of each lesion. The MRI study included pCASL and 3D T1-weighted fat-saturated post-contrast sequences. Of the patients seven were excluded due to technical difficulties or patient movement. The lesions were classified by two raters, blinded to the diagnosis as either hyperperfused or non-hyperperfused, based on the pCASL sequence. The normalized tumor blood flow (nTBF) of each lesion was determined. Qualitative and quantitative characteristics of hypervascular and non-hypervascular lesions were compared.

Results Visual assessment enabled correct classification of 98% of the lesions to be performed. Quantitatively, we found significant differences between the nTBF values for hypervascular and non-hypervascular lesions ($p < 0.001$) and provided cut-off values, allowing meningioma and schwannoma to be distinguished from meningioma and adenoma. Significant differences were also found within the hypervascular group, namely, paraganglioma was more hyperperfused than meningioma ($p = 0.003$) or metastases ($p = 0.009$).

Conclusion The present study demonstrates the high diagnostic performance of pCASL in characterizing skull base lesions by either visual assessment or nTBF quantification. Adding the pCASL sequence to the conventional protocol of skull base assessment can be recommended.

Keywords Arterial spin labeling · Perfusion · Magnetic resonance imaging · Skull base lesions

✉ N. Pyatigorskaya
nadya.pyatigorskaya@aphp.fr

[1] Groupe Hospitalier Pitié-Salpêtrière, Neuroradiology department, AP-HP, 47–83 bd de l'Hôpital, 75651 Paris, France

[2] Radiology department, Ghent University Hospital, Ghent, Belgium

[3] Groupe Hospitalier Pitié-Salpêtrière, Biostatistics Unit, AP-HP, 47–83 bd de l'Hôpital, 75651 Paris, France

[4] UPMC Univ Paris 06 UMR_S1136, and INSERM UMR_S 1136, Institut Pierre Louis d'Epidémiologie et de Santé Publique, Sorbonne Universités, 75013 Paris, France

[5] UPMC Univ Paris 06, Sorbonne Universités, 75013 Paris, France

[6] Groupe Hospitalier Pitié-Salpêtrière, Otology, auditory implants and skull base surgery department, AP-HP, 47–83 bd de l'Hôpital, 75651 Paris, France

Introduction

The differential diagnosis of skull base lesions based on studies by conventional imaging methods can be most challenging. Lesion growth in the skull base largely depends on the angiogenesis process [1]. Perfusion imaging analysis in this region might be helpful in making the correct diagnosis.

Dynamic susceptibility contrast magnetic resonance imaging (DSC-MRI) is clinically the most widespread

technique to study angiogenesis by evaluating tumor perfusion parameters in neuroimaging [2]. Although classical contrast-enhanced perfusion imaging has now become an integral part of the tumor investigation protocol, its use for evaluating extra-axial skull base lesions remains challenging due to susceptibility artifacts caused by field inhomogeneities at the air-bone interface, to which this echo planar acquisition sequence is highly sensitive [3].

Arterial spin labeling (ASL) is a non-invasive MR perfusion technique, in which cerebral blood flow (CBF) is measured by using arterial fluid as a freely diffusible endogenous tracer. No contrast material injection is required [4–6]. By administering a selective inversion pulse, the inflowing spins proximal to the imaging slab are tagged. During the post-labeling delay (PLD), the labeled blood flows into the target tissue in the imaging region and the labeled blood-tissue interaction modifies the tissue relaxation rates. The perfusion contrast is obtained by pair-wise subtraction of the labeled and control unlabeled images [5, 7, 8]. The importance of this technique is currently increasing since it is non-invasive and allows examination of patients with renal impairment. At present, ASL is increasingly incorporated into routine neuroimaging examinations, especially in the case of cerebrovascular pathologies [4, 5, 7–9]. Its applications in non-vascular pathologies, such as tumors or degenerative diseases, are also growing [7].

Pseudo-continuous ASL (pCASL) MRI perfusion can be used as an alternative to DSC-MRI as previous studies have demonstrated a significant correlation between the CBF ratios determined by both techniques. The number of susceptibility artefacts is relatively low in 3D fast spin echo (FSE) pCASL as compared to other ASL methods based on echo-planar imaging (EPI) read-out, which are as prone to susceptibility artefacts as DSC-MRI [10, 11]. Moreover, pCASL provides good labeling efficiency and higher signal-to-noise ratio (SNR) as compared to continuous or pulsed ASL.

The pCASL technique was successfully used with a few small groups of patients for differential diagnosis between cerebellopontine angle schwannoma and meningioma and for predicting perioperative bleeding of pituitary adenomas [12, 13]; however, previous studies were limited to a few types of extra-axial lesions, while less frequent tumors have not yet been investigated. The potential of pCASL-MRI in evaluating different types of skull base lesions and its diagnostic accuracy have not yet been established and properly assessed. The tumor blood flow (TBF) values for most of the skull base lesions, as well as the cut-off values for diagnosis, are still missing in the literature.

In this study, we examined whether the pCASL-MRI perfusion method could be used to adequately assess skull base lesion vascularity and to evaluate its diagnostic performances in detecting hypervascular skull base lesions both qualitatively and quantitatively. Additionally, we intended to provide cut-off values for the differentiation of specific lesion entities.

Materials and Methods

Patients

A total of 99 consecutive patients, examined in the period of September 2014-October 2015, with histologically proven skull base lesions, were retrospectively studied. During this period of time, the pCASL sequence was acquired in every pituitary MRI, and in MRI protocols when a skull base lesion was suspected. The exclusion criteria were the impossibility of acquiring or reading the pCASL sequence because of the patient's movements or agitation or due to technical problems.

To simulate the examination conditions encountered by radiologists in clinical practice and the diagnostic range that radiologists usually consider, the patients were divided into two groups according to the anatomical origin of the lesion. The first group included sellar, suprasellar, and orbital apex lesions. The second group comprised temporal bone, jugular foramen, and cerebellopontine angle lesions.

The study was approved by the local ethical standards committee.

Magnetic Resonance Imaging Studies

The MRI studies were performed using either a 3 Tesla (T) MR (HDxT, GE Healthcare, Milwaukee, WI) whole-body scanner with an 8-channel head coil or a 1.5 T MR (Optima 450 W GEM, GE Healthcare) whole-body scanner with a 16-channel phased-array coil. The imaging protocol included at least pre-contrast ASL perfusion and 3D T1-weighted (T1-w) fat-saturated post-contrast sequence for all patients except one with severe renal function impairment.

The 3D spoiled gradient recalled (SPGR) T1-w fat-saturated sequence was acquired after injecting 0.2 ml/kg body weight of gadolinium (Gd)-DOTA (0.5 M Dotarem, Guerbet, Roissy, France). The parameters used with the 3 T scanner were as follows: TR/TE 9/2.9 ms, NEX 3, receiver bandwidth 19.2 kHz, FOV 24 cm, in-plane resolution 0.75 × 0.94 × 1.2 mm^3, and scan time 4 min 01 sec. In the case of the 1.5 T scanner, the parameters were: TR/TE 17.2/2.4 ms, NEX 2, receiver bandwidth 27.78 kHz, FOV 22 cm, in-plane resolution 0.75 × 0.94 × 1.2 mm^3, and scan time 4 min 03 sec.

The ASL images were acquired using the FSE-pCASL sequence. The automatic labeling process was used. The labeling plane was fixed 2 cm under the imaging slab, parallel to the axial image acquisition plane. Intelligently in-

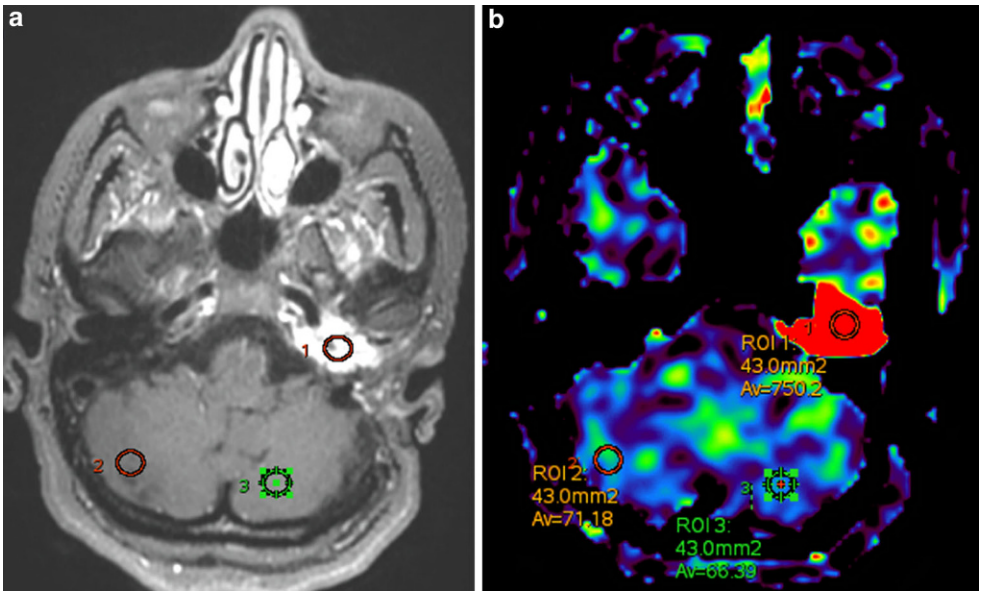

Fig. 1 Determination of the regions of interest. Axial T1-w post-contrast MRI (**a**) shows a homogeneously contrast-enhanced lesion in the left cerebellopontine angle, corresponding to the red colored lesion on the CBF map (**b**). The manually drawn region of interest (ROI) was placed within the largest cross-section of the lesion. The CBF was also measured in two equally sized ROIs in the cerebellar hemispheres. The CBF map demonstrates a highly hypervascular lesion (paraganglioma) with the TBF value of 750.2 ml/100 g/min and the normalized TBF (nTBF) value of 12.9

terwoven spatial saturation pulses, as well as selective and non-selective inversion pulses, were additionally applied to control the magnetization and provide static tissue suppression. The 3 T MRI scanner was employed with the following parameters: TR/TE 4733/9.8 ms, NEX 3, receiver bandwidth 62.5 kHz, post-label delay 2025 ms, FOV 24 cm, spiral acquisition with 8 arms and 512 points per arm, in-plane resolution 3.49 × 3.49 × 4 mm^3, and scan time 4 min 41 sec. With the 1.5 T scanner, the parameters were: TR/TE: 4766/10.7, NEX 3, receiver bandwidth 62.5 kHz, post-label delay 2025 ms, FOV 24 cm, spiral acquisition with 8 arms and 512 points per arm, in-plane resolution 3.7 × 3.7 × 4 mm^3, and scan time 4 min 37 sec. These parameters were fixed in the routine clinical settings.

The volume of blood that flows within the given tissue area per unit time is referred to as CBF and is measured in milliliters of blood per 100 g of tissue per minute (ml/100 g/min) [14]. The CBF maps were calculated using a GE AW workstation (GE Healthcare), as described previously [15], with the READY view post-processing tool.

Image Analysis

***Visual Assessment*:** Two neuroradiologists (1 experienced neuroradiologist with 11 years of experience and 1 radiology resident), blinded to the patients' clinical information, performed subjective tumor perfusion evaluation. In the first part of the process, the raters had to read conventional MRI sequences, being blinded to the pCASL images and then proposed the most likely diagnosis. The suspected diagnosis was rated '0' if the lesion could be included in the supposedly non-hypervascular group on the basis of its appearance as hypoperfused or isoperfused or '1' if the lesion, appearing as hyperperfused, could be included in the supposedly hypervascular group. The raters also proposed the most probable diagnosis (e.g. meningioma, schwannoma). For each analysis, the confidence level was graded from 0 to 4 by each rater. In the second reading, the raters had access to the pCASL sequence with the reconstructed colored CBF maps. The rating was done in the same way as the first one, with '1' standing for hypervascular lesions (if they appeared as hyperperfused) and '0' for non-hypervascular lesions (if they appeared as non-hyperperfused).

***Quantitative Assessment*:** The region of interest (ROI) for the quantitative assessment was drawn at the maximum cross-section of the lesion on the contrast-enhanced fat-suppressed T1-w images. The post-contrast T1-images and CBF maps were automatically co-registered using the vendor-supplied procedure. The absolute TBF (aTBF) value was calculated within the ROI. Since cystic, necrotic and hemorrhagic tumor components lead to TBF underestimation, these regions were avoided in the ROI placement. To obtain normalized TBF (nTBF) values, the tumor to healthy tissue perfusion ratios were calculated by dividing the mean value of the circular tumor ROI by the mean value of two equally sized ROIs in the bilateral cerebellar hemispheres (Fig. 1), as described previously [3, 16].

Diagnostic Confirmation

All the lesions were analyzed by an experienced senior anatomopathologist with 16 years of experience. Each of the included patients had a histopathological confirmation of the lesion nature. According to the final histological diagnosis for each patient and on the basis of

Table 1 Characteristics of the patients

	Pituitary, suprasellar, orbital apex[b]			Temporal bone, jugular foramen, cerebellopontine angle[b]		
Hypervascularization[a] (yes = 1, no = 0)	1	0	*p*-value	1	0	*p*-value
Number of patients	17	15	–	34	26	–
Age (years)	56.0 (44.0–71.0)	43.0 (30.5–68.0)	$p = 0.23$	63.0 (58.3–73.5)	56.0 (42.0–67.0)	$p = 0.06$
Gender (men/women)	11/6	4/11	–	18/16	15/11	–
Characterization	17/17 (100%)	15/15 (100%)	–	34/34 (100%)	24/26 (92%)	–
nTBF (median/IQR)	3.56 (3.05–5.35)	0.68 (0.26–0.92)	$p < 0.0001$	5.42 (3.37–10.63)	0.71 (0.45–0.91)	$p < 0.0001$
aTBF (median/IQR)[c]	152.40 (132.48–217.5)	34.0 (13.73–46.59)	$p < 0.0001$	285.55 (163.50–524.6)	35.68 (23.85–43.74)	$p < 0.0001$

IQR interquartile range, *nTBF* normalized blood flow in tumor, *aTBF* absolute blood flow in tumor
[a] Characterization as hyperperfused or non-hyperperfused
[b] The anatomical locations are detailed in Table 2 and 3
[c] ml/min/100 g

Table 2 Characterization of pituitary, suprasellar and orbital apex region lesions

Hypervascularization		Number	Characterization[a] (correct/total)	nTBF (median/IQR)	aTBF (median/IQR) (ml/min/100 g)
Hypervascular lesions[b]	Metastasis	3	3/3 (100%)	3.30 (2.70–4.51)	150.5 (121.47–32.25)
	Meningioma	14	14/14 (100%)	3.82 (3.07–5.28)	172.95 (134.26–216.85)
Non-hypervascular lesions[b]	Rathke's cleft cyst	2	2/2 (100%)	0.43 (0.31–0.56)	21.44 (15.16–27.72)
	Adenoma	13	13/13 (100%)	0.78 (0.34–0.95)	34.57 (15.37–47.73)

IQR interquartile range, *nTBF* normalized blood flow in tumor, *aTBF* absolute blood flow in tumor
[a] Characterization as hyperperfused/non-hyperperfused
[b] Significant differences between hypervascular and non-hypervascular lesions ($p < 0.0001$)

numerous previous studies on the vascularity of different tumor types [3, 17–29], the lesions were classified as hypervascular (meningioma, metastasis, paraganglioma, hemangioblastoma, temporal bone infection, plasmacytoma, and endolymphatic sac tumor) or non-hypervascular (schwannoma, adenoma, chondrosarcoma, cholesteatoma, pseudotumor, and Rathke's cleft cyst).

Statistical Analysis

The data are presented in terms of median and interquartile range (IQR) for quantitative variables and percent in the case of qualitative assessment. Statistical analysis software (SAS) (version 9.3; SAS Institute, Cary, NC) was used. All tests were two-sided.

The kappa coefficient was used to assess the inter-rater agreement. The raters' evaluations of each lesion classification (as hypervascular or as non-hypervascular) were compared with the classification based on the histological diagnosis using the McNemar's test. The non-parametric Kruskall Wallis test was used for quantitative comparison between hypervascular and non-hypervascular lesions and also between different hypervascular lesions (temporal bone, jugular foramen, and cerebellopontine angle lesions). In the latter case, the global test was followed by the post hoc pair-wise comparison for the lesion number $n \geq 3$, performed by means of the Dwass-Steel-Chritchlow-Fligner correction for multiple comparisons. The diagnostic threshold value was calculated using receiver operating characteristic (ROC) curve analysis. The sensitivity and specificity of the cut-off points were estimated using the Youden index. The $p < 0.05$ values were considered significant.

Results

A total of 92 patients with a mean age of 57.4 ± 17.7 and including 48 men (52%) were included in the study (Table 1). According to the histological analysis, 51 patients presented with hypervascular lesions and 41 patients presented with non-hypervascular lesions. The lesions were: meningiomas ($n = 21$), pituitary adenomas ($n = 13$), schwannomas ($n = 12$), paragangliomas ($n = 10$), metastasis ($n = 9$), infections ($n = 5$), pseudotumors ($n = 4$), cholesteatomas ($n = 3$), chondrosarcomas ($n = 3$), hemangioblastomas ($n = 3$), lymphomas ($n = 3$), plasmacytomas ($n = 2$), Rathke's cleft cysts

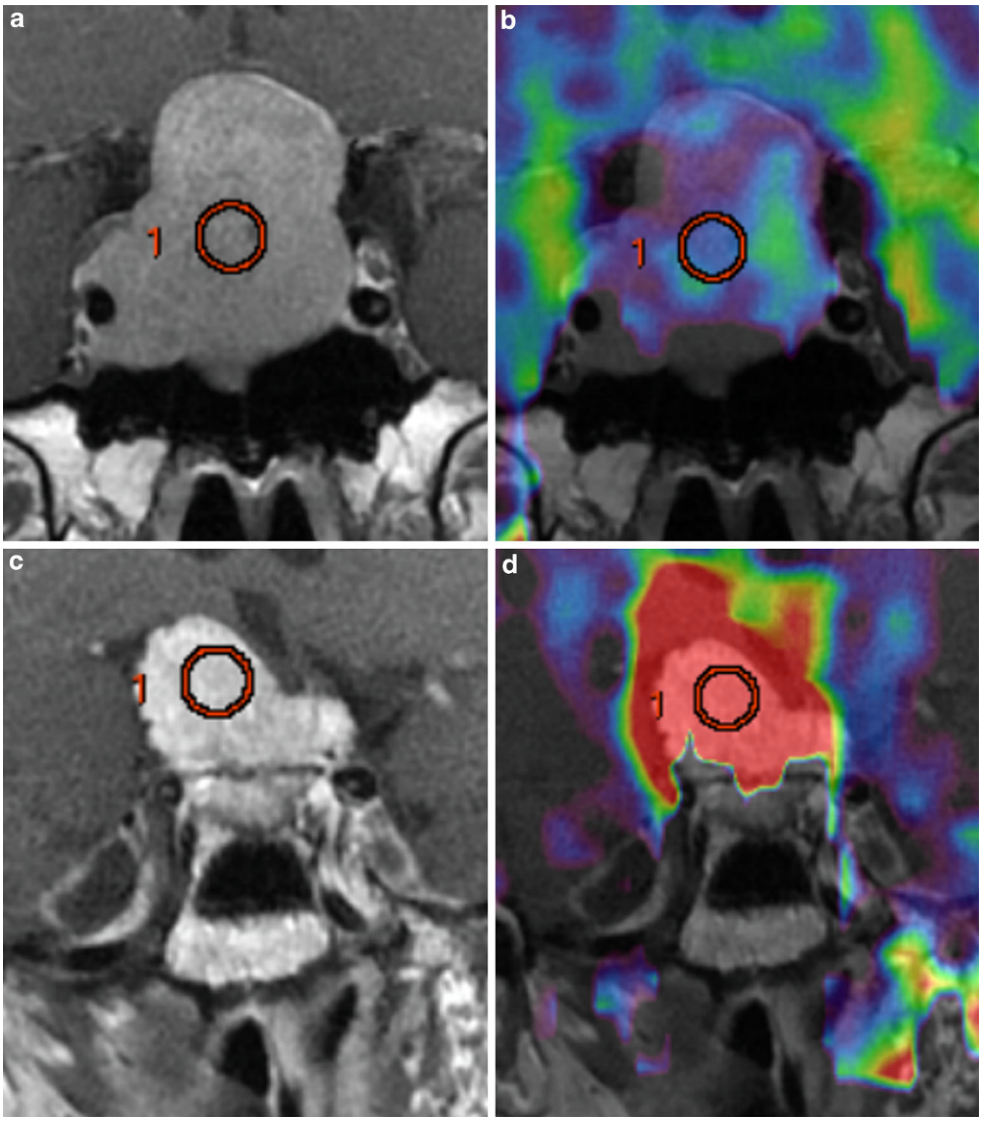

Fig. 2 Characterization of pituitary region lesions: pituitary adenoma and meningioma. Coronal T1-w post-contrast MRI (**a**, **c**) shows two homogeneously contrast-enhanced lesions in the pituitary region. The CBF map shows a non-hyperperfused lesion (**b**) with a low tumor to healthy tissue perfusion ratio (nTBF = 0.82), corresponding to pituitary adenoma. As observed on the CBF map (**d**), the hyperperfused lesion with high tumor to healthy tissue ratio (nTBF = 5.35), corresponds to meningioma

(n = 2), cystic lymphangioma (n = 1), and endolymphatic sac tumor (n = 1). Of the patients seven were excluded from the study due to motion artefacts (n = 3) and/or the impossibility of post-processing the pCASL sequence, which was erroneously marked as being acquired or had indeed been acquired after contrast injection (n = 4).

Diagnostic Performance of the pCASL Method

Out of 92 lesions 90 were correctly characterized visually as hypervascular or non-hypervascular by both raters using the pCASL sequence. An excellent interrater reliability was observed, with the kappa coefficient of 0.95 (95% confidence interval CI = 0.89–1). The diagnostic confidence level assessed by both raters was high, with the maximum value of 4 for 84 (91%) lesions. The mean sensitivity over 2 raters was 1, the specificity was 0.95, the positive predictive value was 0.96, and the negative predictive value was 1. By adding the pCASL sequence to the conventional assessment, the number of correct classifications increased from 81% to 98% ($p < 0.001$). The mean diagnostic confidence increased by one point (from 2.6 ± 1.89 to 3.87 ± 0.44).

Visually, TBF maps obtained from 1.5 T and 3 T MR scans were of similar quality and no significant differences between the 3 T and 1.5 T nTBF values ($p = 0.68$) were observed. There were not more technical failures of the ASL sequence acquisition at 1.5 T than at 3 T. Quantitative analysis showed that the nTBF values were significantly higher in hypervascular lesions (median: 4.48, IQR = 3.29–8.32) as compared to non-hypervascular lesions (median: 0.71, IQR = 0.34–0.92, $p < 0.0001$). The cut-off nTBF value between all the hypervascular and non-hypervascular lesions varied in the interval of 1.84–1.88. Hypervascular lesions

Table 3 Temporal bone, jugular foramen and cerebellopontine angle lesions

Hypervascularization		Number	Characterization[a] (correct/total)	nTBF (median/IQR)	aTBF (median/IQR) (ml/min/100 g)
Hypervascular lesions[b]	Metastasis[d]	6	6/6 (100%)	3.31 (3.10–4.57)	196.80 (135.25–255.80)
	Infection	5	5/5 (100%)	3.39 (2.54–3.86)	129.80 (105.40–143.30)
	Meningioma[c]	7	7/7 (100%)	3.39 (3.33–4.16)	168.0 (153.75–201.30)
	Plasmacytoma	2	2/2 (100%)	5.38 (4.42–6.34)	242.10 (209.65–274.55)
	Endolymphatic sac tumor	1	1/1 (100%)	5.82 (5.82–5.82)	304.90 (304.90–304.90)
	Paraganglioma[c, d]	10	10/10 (100%)	10.88 (9.32–13.13)	602.50 (472.3–768.98)
	Hemangioblastoma	3	3/3 (100%)	11.73 (10.03–17.48)	448.40 (421.30–776.70)
Non-hypervascular lesions[b]	Cholesteatoma	3	3/3 (100%)	0.19 (0.14–0.34)	4.80 (4.51–12.70)
	Cystic lymphangioma	1	1/1 (100%)	0.33 (0.33–0.33)	15.90 (15.90–15.90)
	Pseudotumor	4	4/4 (100%)	0.55 (0.32–0.80)	24.21 (20.19–29.96)
	Chondrosarcoma	3	3/3 (100%)	0.67 (0.62–0.75)	37.54 (36.81–38.15)
	Schwannoma	12	12/12 senior (100%) 10/12 junior (83%)	0.75 (0.62–1.02)	35.68 (29.51–50.35)
	Lymphoma	3	3/3 (100%)	1.44 (1.42–1.48)	54.41 (47.14–56.10)

IQR Interquartile Range, *nTBF* normalized blood flow in tumor, *aTBF*: absolute blood flow in tumor

[a] Characterization as hyperperfused/non hyperperfused, [b] Significant differences between hypervascular and non-hypervascular lesions ($p < 0.0001$)

[c] Significant difference between paraganglioma and meningioma ($p = 0.003$)

[d] Significant difference between paraganglioma and metastasis ($p = 0.009$)

also displayed significantly higher aTBF values than non-hypervascular lesions (Table 1) although the two groups overlapped. The ROC analysis was performed and the best Youden index was achieved for the aTBF threshold of 86.9, the sensitivity and the specificity being 98% and 100%, respectively.

Characterization of Pituitary, Suprasellar, and Orbital Apex Region Lesions

Of the patients 32 presented with pituitary, suprasellar, or orbital apex-region lesions (Table 2). All the lesions were correctly characterized by both visual assessment and quantitative pCASL analysis (Table 2). There was a significant difference in the nTBF values for the hypervascular and the non-hypervascular groups ($p < 0.0001$) (Table 1). The calculated cut-off nTBF values, which can be used to differentiate hypervascular and non-hypervascular lesions were 1.25–2.04. Remarkably, meningiomas could be correctly distinguished from adenomas based on both visual assessment (Fig. 2) and quantitative analysis (Fig. 3a).

Characterization of Temporal Bone, Jugular Foramen, and Cerebellopontine Angle Lesions

A total of 60 patients presented with temporal bone, jugular foramen, or cerebellopontine angle lesions. (Table 3). Based on visual assessment, all the lesions except for two schwannomas, were correctly characterized, while quantitative analysis led to correct characterization of all the lesions (Table 3). The quantitative analysis showed significant difference between the nTBF values for the hypervascular and non-hypervascular lesions ($p < 0.0001$) (Table 1). All hypervascular and non-hypervascular lesions could be differentiated (with the cut-off values 1.84–1.88): e.g. meningiomas were successfully distinguished from schwannomas and paragangliomas were successfully distinguished from chondrosarcomas both by visual assessment (Figs. 4 and 5) and by quantitative measurements (Fig. 3b).

Characterization of Hyper-vascular Lesions

The Kruskall Wallis test showed significant differences between the nTBF results within the hyper-vascular group ($p = 0.009$). Pair-wise comparisons (Table 3; Fig. 3b) showed

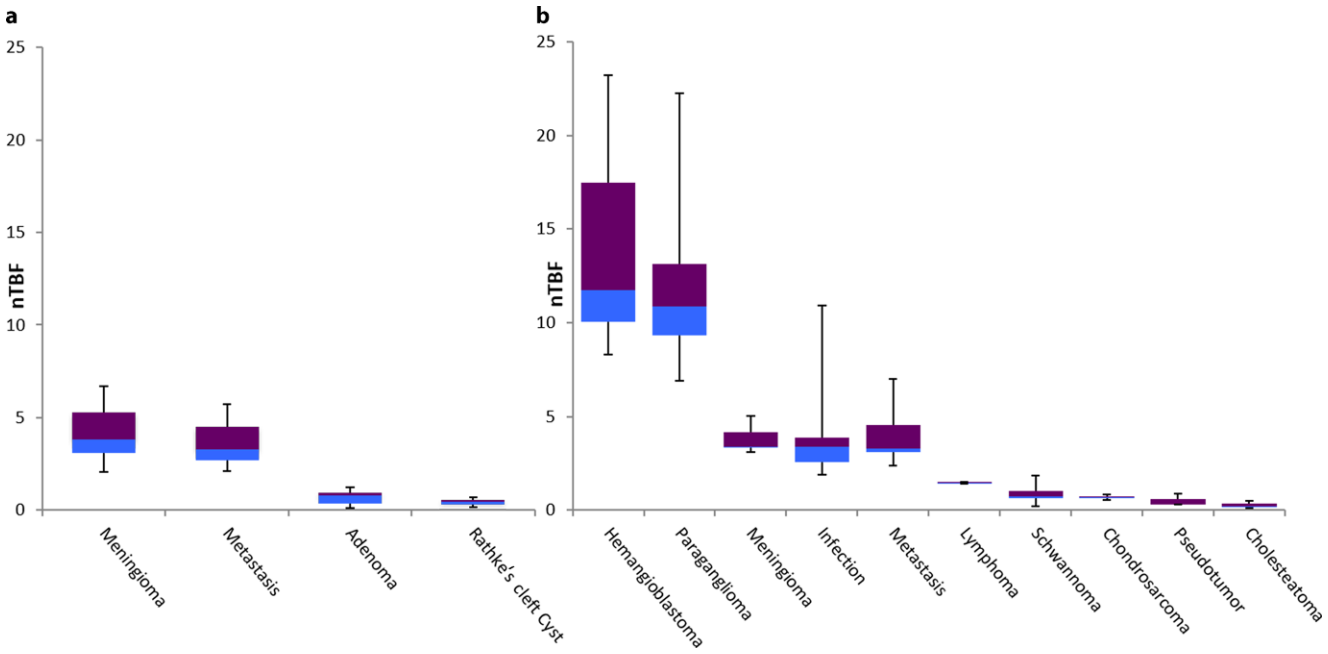

Fig. 3 Boxplots of the normalized tumor blood flow. The boxplots shows the nTBF values for different skull base lesions in the pituitary, suprasellar, and orbital apex regions (**a**) and in the temporal bone, jugular foramen, and cerebellopontine angle (**b**)

significant differences between meningiomas and paragangliomas ($p = 0.003$) as well as between metastasis and paragangliomas ($p = 0.009$). In contrast to this, no significant differences were found between meningiomas and infections ($p = 0.94$) or between meningioma and metastasis ($p = 0.89$). The number of cases for plasmacytomas and endolymphatic sac tumor were too small for their pair-wise comparison.

Discussion

In the present study, we demonstrated that pCASL images could be successfully used for differentiating with excellent diagnostic accuracy between hypervascular and non-hypervascular skull base lesions both by means of visual assessment and by quantitative measurements of perfusion ratios. Moreover, we demonstrated the high diagnostic performance of the method in differentiating common lesions in specific locations, in particular, meningiomas from adenomas (sellar region) and paragangliomas from chondrosarcomas (petrous region). The quantitative approach can be used not only for reliable differentiation between hypervascular and non-hypervascular lesions, but has also proved to be highly effective in distinguishing different types of lesions according to their degree of hyperperfusion.

pCASL Sequence in Skull Base Imaging

Perfusion assessment is known to be widely used not only for stroke evaluation, but also as an important biological parameter of tumor characterization [11, 30, 31]. While contrast enhancement allows assessment of blood brain barrier disruption, perfusion measurements make it possible to assess the lesion microvascularization and neoangiogenesis [7, 13, 32]. The ASL procedure is already used for assessing CBF in the case of brain tumors as well as cerebrovascular and degenerative diseases [8]. It was also shown to be an effective alternative to the DSC-MRI method [3, 12, 19, 33, 34] and even to provide more reproducible results of blood flow measurements than DSC-MRI [8]. The pCASL sequence was chosen due to its high labeling efficiency. As compared to other ASL methods, the pCASL sequence is strongly recommended for the purpose of clinical imaging [3]. Moreover, since the spin-echo-based pCASL is less prone to susceptibility artefacts, this method can solve the problem of susceptibility artefacts caused by field inhomogeneities at the air-bone interface in skull base imaging [3]; however, when acquiring and reading the pCASL sequence, the possible presence of motion artifacts should be kept in mind. Additionally, the correct positioning of the labeling plane is essential since the labeling efficiency may be altered when the labeling plane is in the region of magnetic field inhomogeneities, such as dental material, which results in inaccurate CBF maps [5, 7]. The relatively long PLD of 2025 ms was chosen because of the greater arterial transit

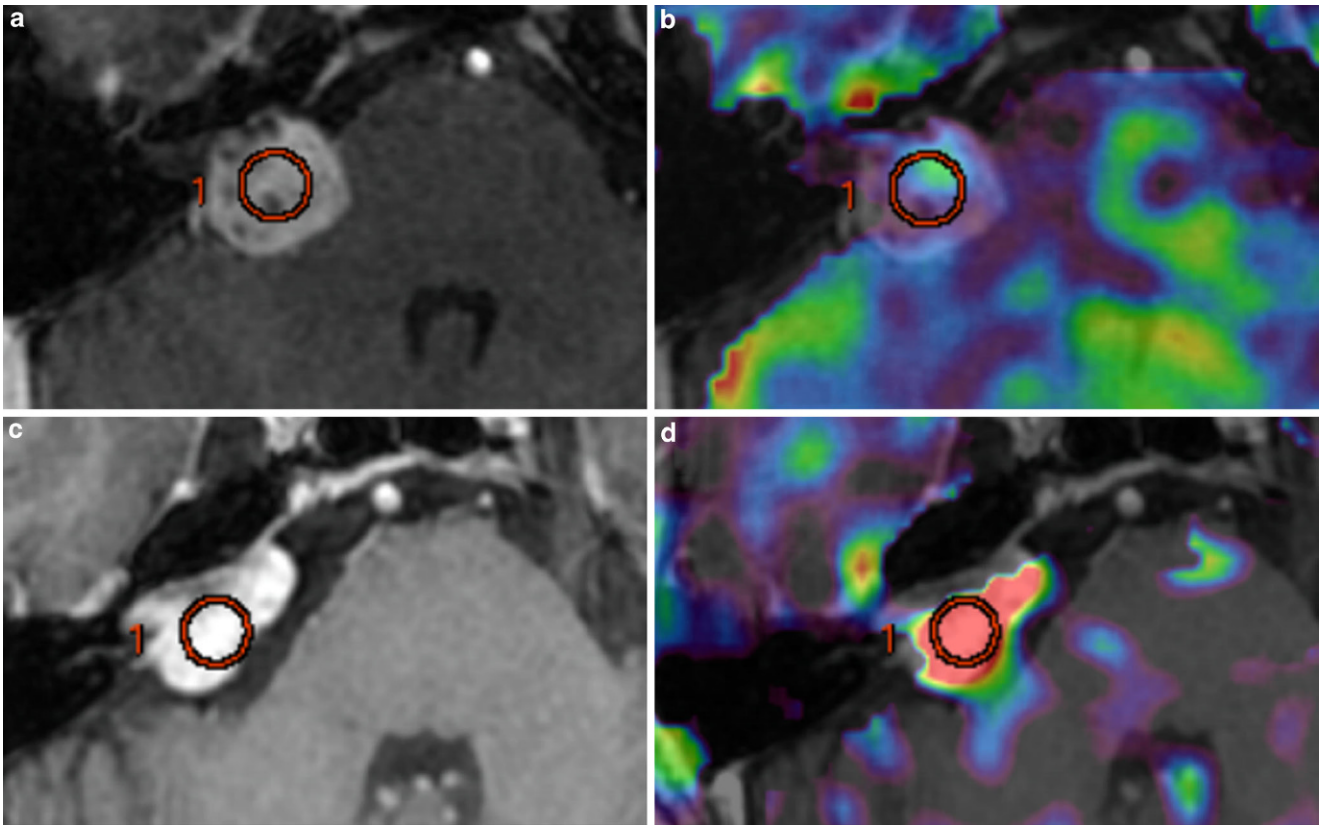

Fig. 4 Characterization of cerebellopontine angle lesions: schwannoma and meningioma. The axial fat-suppressed post-contrast T1-w MRI (**a**, **c**) shows two contrast-enhanced lesions in the right cerebellopontine angle. The calculated CBF map reveals a non-hyperperfused schwannoma (nTBF = 0.85) (**b**) and a hyperperfused meningioma (nTBF = 3.29) (**d**)

times between the labeling plane and the target tissue in the skull base region [35].

pCASL Sequence in Skull Base Tumor Imaging

It was reported that the DSC-MRI method could be used to differentiate meningiomas from schwannomas due to the vascular character of the former [18]. The ASL and DSC-MRI studies of meningiomas provided comparable results [8]. Previously, the ASL-TBF maps allowed differentiation of schwannomas from meningiomas based on their perfusion characteristics [3, 13–17]. Our study not only confirms these previous findings, but also shows that both visual assessment and quantitative measurements allow differentiation between the two abovementioned lesion types. The TBF assessment increases the diagnostic accuracy and confidence as compared to the classically described morphological features, such as the pattern of contrast enhancement, the presence of dural enhancement and tumor location relative to other anatomical structures. In the present study, two schwannomas were incorrectly classified by the junior radiologist, which can be due to the small lesion size and slightly higher TBF in some schwannomas; however, the senior radiologist and the quantitative analysis could correctly classify all the lesions. Furthermore, based on morphological imaging, chondrosarcomas of the jugular foramen can sometimes be misdiagnosed as paragangliomas or as endolymphatic sac tumors [36]. We believe that pCASL makes it possible to easily differentiate these lesions because chondrosarcomas appear as non-hyperperfused, while both paraganglioma [37] and endolymphatic sac tumors [22] are strongly hyperperfused. Similar perfusion differences were observed between chondrosarcomas and plasmacytomas, with much higher TBF values in the latter tumors.

As for the pituitary region, the ASL sequence effectiveness in predicting post-operative hemorrhage in pituitary adenoma was previously assessed [12], but the ASL potential for differential diagnosis of skull base tumors has not yet been studied. Our results demonstrate that, despite individual perfusion variations in adenomas, this tumor can be successfully differentiated from meningiomas by means of pCASL, both visually and quantitatively, since meningiomas are highly hyperperfused, while adenomas are non-perfused or weakly perfused. In addition, while differentiating pituitary adenoma from metastases can be challenging on conventional imaging [38], pCASL is advantageous in

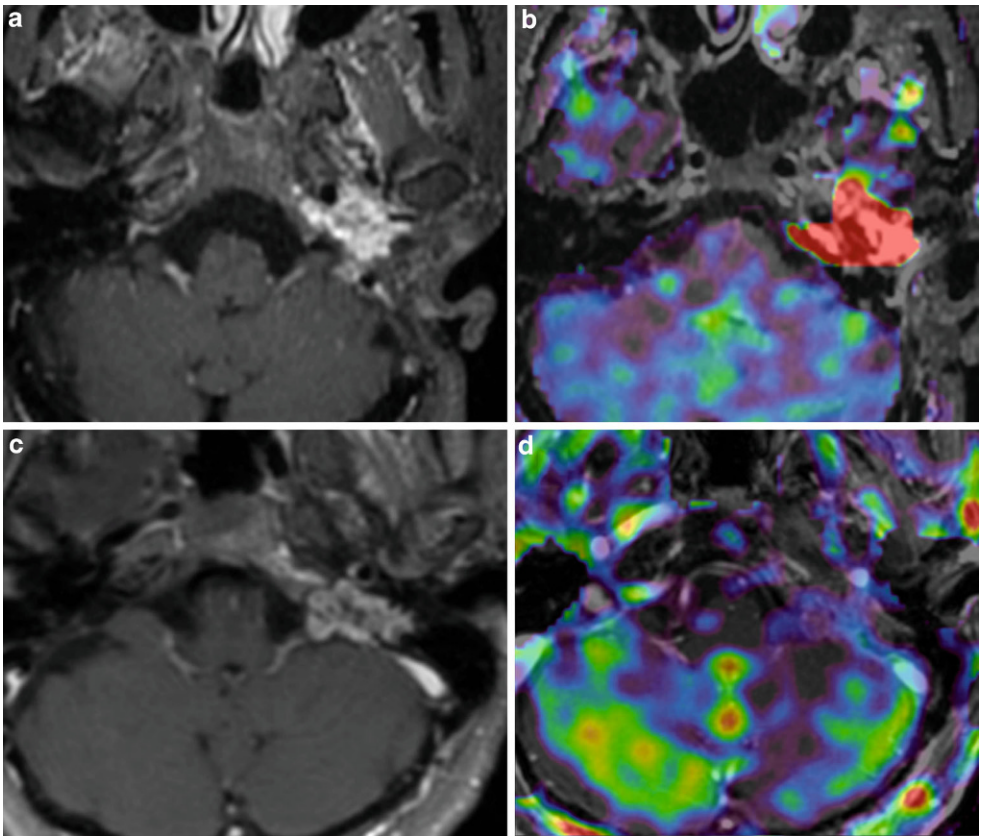

Fig. 5 Characterization of the lesions in the jugular foramen region. The axial post-contrast fat-saturated T1-w images show two different heterogeneously contrast-enhanced lesions in the left jugular foramen region (**a**, **c**). The fusion between the post-contrast fat-saturated T1-w image and the CBF map reveal a markedly hyperperfused paraganglioma (nTBF = 6.9) (**b**) and a non-hyperperfused pattern of chondrosarcoma (nTBF = 0.56) (**d**)

this case since metastases (in our case, originating from the lungs) appears to be more hyperperfused than adenoma.

Besides being highly advantageous in differentiating hypervascular from non-hypervascular lesions, pCASL can be successfully used to separate different types of hypervascular lesions according to their degree of hypervascularization. In particular, this technique is effective in differentiating paragangliomas from other lesions, such as meningiomas or metastases, because the former have significantly higher TBF values than the latter. We have also found very high TBF values for hemangioblastomas, in line with previous studies [13], with large cut-off values as compared to meningioma or metastases. At the same time, we were not able to differentiate metastases and meningiomas based on the pCASL images, in line with the previously reported metastasis study [13]; however, it should be taken into account that perfusion of metastases can vary according to their histological type.

To the best of our knowledge, the present study is the first one reporting ASL perfusion results in plasmacytoma, endolymphatic sac tumor, chondrosarcoma, cholesteatoma, and pseudo-tumor. For this reason, our results could not be compared to previous literature data concerning the ASL perfusion. Nevertheless, correlation between ASL signal and histological vessel density was previously demonstrated [13] and previous pathological and imaging studies can be considered to support our findings. For example, chondrosarcomas [39], cholesteatomas [42], and pseudo-tumors [43] are known to be non-hyperperfused lesions, while plasmacytomas or endolymphatic sac tumors [22] are usually hyperperfused. In this study, we determined TBF values for lesions where perfusion was previously poorly assessed; however, they should still be confirmed in large scale studies.

Using pCASL does not allow differentiation of benign from malignant lesions since vascularity alone is not a sufficient criterion. Indeed, several histologically benign lesions appear to be hypervascular with high nTBF (e. g. meningiomas or paragangliomas), while some malignant lesions (e. g. chondrosarcomas) appear to be non-hypervascular, with low nTBF.

pCASL Sequence in Skull Base Osteitis Imaging

We did not succeed in differentiating skull base osteitis from metastatic lesions or meningiomas, all of which were characterized by a hyperperfusion pattern on pCASL. While this can be considered as a limitation, the radiological aspect of these lesions was well recognizable. Thus, it appears that pCASL may be a valuable alternative to contrast agent injection imaging in assessing malignant otitis, especially in diabetic patients with renal impairment, for whom con-

trast agent injection is usually avoided. Moreover, taking into account that the long-term consequences of repeated gadolinium-based contrast-agent injections are still controversial [40], contrast-free methods appear even more valuable. This is especially important for children, for lesions that require repeated follow-up examinations [41], and for the prevention of nephrogenic systemic fibrosis in patients with severe renal failure [40].

Absolute and Relative TBF Measurements in pCASL Imaging

As has been mentioned ASL allows quantitative measurements of CBF, which are assumed to be independent of the sequence parameters. Thus, aTBF values can be analyzed directly or normalized with respect to the normal structure (nTBF);however, different CBF values were reported in the literature, especially when obtained with different sequence parameters [42]. The variability appears lower with the pCASL sequence, which is now recommended in clinical practice [43]. In skull base lesions, normalization of TBF remains problematic since comparison with the contralateral normal side is often impossible. In several previous studies, it was suggested to normalize the TBF values with respect to pterygoid muscles [11] or cerebellar hemispheres [3, 16]. We have chosen the latter option since cerebellar hemispheres, unlike pterygoids, were always included in the acquisition volume. We chose nTBF rather than aTBF values because we observed that they provided better tumor characterization with a clear cut-off between the hypervascular and non-hypervascular lesions; however, aTBF values also allowed correct characterization of the lesions, with excellent sensitivity and specificity. Moreover, the TBF values obtained in our study were consistent with those previously reported, especially for meningiomas and schwannomas [17]. This finding suggests that ASL gives reproducible results with different MR scanners; however, the reproducibility of ASL sequences obtained with scanners from other vendors still has to be shown. So far, there are relatively few data in the literature [17] to support our quantitative results concerning perfusion of skull base lesions as assessed by ASL or other perfusion methods [8, 17]. Largescale multicenter studies are needed to confirm our results.

Study Limitations

There are a few limitations to the present study. While the overall number of included lesions was high, some lesions were poorly represented because of their low prevalence. In addition, the small number of some lesions, such as metastases, did not allow comparison with different histological types. This comparison could be interesting since some histological types of metastases (e. g. melanoma or renal cell carcinoma) are expected to be strongly hyperperfused, while others (e. g. colon) are expected to be less hyperperfused [44]. Further studies with a larger number of metastases are needed to investigate this point. Furthermore, some of the lesions were screened using the 1.5 T scanner, which was not in line with recent recommendations for ASL [15]. At high strength of the magnetic field the T1 length increases, which leads to the SNR growth. On the other hand, 3 T has more susceptibility to field inhomogeneities as compared to 1.5 T [41]; however, there were no significant differences in the measurements of similar lesions performed with the two scanners, which is in agreement with previous reports of reproducible CBF values obtained with 1.5 T and 3 T imaging [15]. We did not observe higher probability of sequence acquisition failure at 1.5 T, either. Finally, although the histopathological study comprised the assessment of a hypervascular versus non-hypervascular patterns, it was not specifically intended for a vascular count. Nevertheless, by means of the TBF analysis, correct classification of all the lesions, consistent with the global pathological diagnosis, was achieved. Moreover, the correlation between the ASL CBF and vascular count results has already been demonstrated in previous studies [8, 13, 17].

Conclusion

The present study demonstrated the high diagnostic performance of the pCASL method in characterizing skull base lesions by means of either visual assessment or nTBF quantification. While visual assessment allows easy differentiation between hypervascular and non-hypervascular lesions, quantitative analysis is even more accurate, allowing finer distinction between different hypervascular lesions. Based on these results, it can be recommended that pCASL sequence should be added to the conventional protocol of skull base assessment. Additional studies comparing the post-contrast acquisition to the pCASL sequence are needed to determine whether the pCASL technique can be successfully used for lesion characterization when contrast administration should be avoided.

Acknowledgements Special acknowledgements to Marion Uettwiller for her assistance with certain technical aspects of the pCASL sequence.

Compliance with ethical guidelines

Conflict of interest B. Geerts, D. Leclercq, S. Tezenas du Montcel, B. Law-ye, S. Gerber, D. Bernardeschi, D. Galanaud, D. Dormont and N. Pyatigorskaya declare that they have no competing interests.

Ethical standards All procedures performed in studies involving human participants were in accordance with the ethical standards of the institutional and/or national research committee and with the 1964 Helsinki declaration and its later amendments or comparable ethical standards. Informed consent was obtained from all individual participants included in the study.

References

1. Folkman J. Seminars in Medicine of the Beth Israel, Boston. Clinical applications of research on angiogenesis. N Engl J Med. 1995;333:1757–63.
2. Boxerman JL, Shiroishi MS, Ellingson BM, Pope WB. Dynamic Susceptibility Contrast MR Imaging in Glioma. Review of current clinical practice. Magn Reson Imaging Clin N Am. 2016;24:649–70.
3. Järnum H, Steffensen EG, Knutsson L, Fründ ET, Simonsen CW, Lundbye-Christensen S, Shankaranarayanan A, Alsop DC, Jensen FT, Larsson EM. Perfusion MRI of brain tumours: a comparative study of pseudo-continuous arterial spin labeling and dynamic susceptibility contrast imaging. Neuroradiology. 2010;52:307–17.
4. Hartkamp NS, van Osch MJ, Kappelle J, Bokkers RP. Arterial spin labeling magnetic resonance perfusion imaging in cerebral ischemia. Curr Opin Neurol. 2014;27(1):42–53.
5. Deibler AR, Pollock JM, Kraft RA, Tan H, Burdette JH, Maldjian JA. Arterial Spin-labeling in routine clinical practice, part 1: technique and artifacts. AJNR Am J Neuroradiol. 2008;29:1228–34.
6. Brendle C, Hempel JM, Schittenhelm J, Skardelly M, Tabatabai G, Bender B, Ernemann U, Klose U. Glioma Grading and Determination of IDH Mutation Status and ATRX loss by DCE and ASL Perfusion. Clin Neuroradiol. 2017. https://doi.org/10.1007/s00062-017-0590-z
7. Grade M, Hernandez Tamames JA, Pizzini FB, Achten E, Golay X, Smits M. A neuroradiologist's guide to arterial spin labeling MRI in clinical practice. Neuroradiology. 2015;57:1181–202.
8. Kimura H, Takeuchi H, Koshimoto Y, Arishima H, Uematsu H, Kawamura Y, Kubota T, Itoh H. Perfusion imaging of meningioma by using continuous arterial spin-labeling: comparison with dynamic susceptibility-weighted contrast-enhanced MR images and histopathologic features. AJNR Am J Neuroradiol. 2006;27:85–93.
9. Amukotuwa SA, Yu C, Zaharchuk G. 3D pseudocontinuous arterial spin labeling in routine clinical practice: a review of clinically significant artifacts. J Magn Reson Imaging. 2016;43:11–27.
10. Wong AM, Yan FX, Liu HL. Comparison of three-dimensional pseudo-continuous arterial spin labeling perfusion imaging with gradient-echo and spin-echo dynamic susceptibility contrast MRI. J Magn Reson Imaging. 2014;39:427–33.
11. Fujima N, Kudo K, Tsukahara A, Yoshida D, Sakashita T, Homma A, Tha KK, Shirato H. Measurement of Tumor Blood Flow in Head and Neck Squamous Cell Carcinoma by Pseudo-Continuous Arterial Spin Labeling: Comparison With Dynamic Contrast-Enhanced MRI. J Magn Reson Imaging. 2015;41:983–91.
12. Sakai N, Koizumi S, Yamashita S, Takehara Y, Sakahara H, Baba S, Oki Y, Hiramatsu H, Namba H. Arterial Spin-Labeled Perfusion Imaging Reflects Vascular Density in Nonfunctioning Pituitary Macroadenomas. AJNR Am J Neuroradiol. 2013;34:2139–43.
13. Noguchi T, Yoshiura T, Hiwatashi A, Togao O, Yamashita K, Nagao E, Shono T, Mizoguchi M, Nagata S, Sasaki T, Suzuki SO, Iwaki T, Kobayashi K, Mihara F, Honda H. Perfusion imaging of brain tumors using arterial spin-labeling: correlation with histopathologic vascular density. AJNR Am J Neuroradiol. 2008;29:688–93.
14. Griffith B, Jain R. Perfusion Imaging In Neuro-Oncology: Basic Techniques and Clinical Applications. Radiol Clin North Am. 2015;53:497–511.
15. Alsop DC, Detre JA, Golay X, Günther M, Hendrikse J, Hernandez-Garcia L, Lu H, MacIntosh BJ, Parkes LM, Smits M, van Osch MJ, Wang DJ, Wong EC, Zaharchuk G. Recommended implementation of arterial spin-labeled perfusion MRI for clinical applications: A consensus of the ISMRM perfusion study group and the European consortium for ASL in dementia. Magn Reson Med. 2015;73:102–16.
16. Arbab AS, Aoki S, Toyama K, Kumagai H, Arai T, Kabasawa H, Takahashi Y, Araki T. Brain perfusion measured by flow-sensitive alternating inversion recovery (FAIR) and dynamic susceptibility conrast-enhanced magnetic resonance imaging: comparison with nuclear medicin technique. Eur Radiol. 2001;11:635–41.
17. Yamamoto T, Takeuchi H, Kinoshita K, Kosaka N, Kimura H. Assessment of tumor blood flow and its correlation with histopathologic features in skull base meningiomas and schwannomas by using pseudo-continuous arterial spin labeling images. Eur J Radiol. 2014;83:817–23.
18. Maeda M, Itoh S, Kimura H, Iwasaki T, Hayashi N, Yamamoto K, Ishii Y, Kubota T. Vascularity of meningiomas and neuromas: assessment with dynamic susceptibility-contrast MR imaging. AJR Am J Roentgenol. 1994;163:181–6.
19. Jiang J, Zhao L, Zhang Y, Zhang S, Yao Y, Qin Y, Wang CY, Zhu W. Comparative analysis of arterial spin labeling and dynamic susceptibility contrast perfusion imaging for quantitative perfusion measurements of brain tumors. Int J Clin Exp Pathol. 2014;7:2790–9.
20. van den Berg R. Imaging and management of head and neck paragangliomas. Eur Radiol. 2005;15:1310–8.
21. Bush ML, Pritchett C, Packer M, Ray-Chaudhury A, Jacob A. Hemangioblastoma of the cerebellopontine angle. Arch Otolaryngol Head Neck Surg. 2010;136:734–8.
22. Sun YH, Wen W, Wu JH, Song JM, Guan H, Wang KX, Xu MQ. Endolymphatic sac tumor: case report and review of the literature. Diagn Pathol. 2012;7:36.
23. Chang PC, Fischbein NJ, Holliday RA. Central Skull Base Osteomyelitis in Patients without Otitis Externa: Imaging Findings. AJNR Am J Neuroradiol. 2003;24:1310–6.
24. Ginat DT, Bokhari A, Bhatt S, Dogra V. Inflammatory pseudotumors of the head and neck in pathology-proven cases. J Neuroradiol. 2012;39:110–5.
25. Guo SY, Cai XQ, Ma J, Wang WY, Lu G. Diagnosis of concomitant pituitary adenoma and Rathke's cleft cyst with magnetic resonance imaging. Int J Surg. 2015;18:191–5.
26. Kothary N, Law M, Cha S, Zagzag D. Conventional and perfusion MR imaging of parafalcine chondrosarcoma. AJNR Am J Neuroradiol. 2003;24:245–8.
27. Corrales CE, Fischbein N, Jackler RK. Imaging Innovations in Temporal Bone Disorders. Otolaryngol Clin North Am. 2015;48:263–80.
28. Akkari M, Gabrillargues J, Saroul N, Pereira B, Russier M, Mom T, Gilain L. Contribution of magnetic resonance imaging to the diagnosis of middle ear cholesteatoma: Analysis of a series of 97 cases. Eur Ann Otorhinolaryngol Head Neck Dis. 2014;131:153–8.
29. Cerase A, Tarantino A, Gozzetti A, Muccio CF, Gennari P, Monti L, Di Blasi A, Venturi C. Intracranial involvement in plasmacytomas and multiple myeloma: a pictorial essay. Neuroradiology. 2008;50:665–74.
30. Siemonsen S, Fitting T, Thomalla G, Krützelmann A, Fiehler J. Visual assessment of magnetic resonance imaging perfusion lesions in a large patient group. Clin Neuroradiol. 2012;22:305–13.
31. Turowski B, Schramm P. An Appeal to Standardize CT-and MR-Perfusion. Clin Neuroradiol. 2015;25 Suppl 2:205–10.
32. Radbruch A, Bendszus M. Advanced MR Imaging in Neuro-oncology. Clin Neuroradiol. 2015;25 Suppl 2:143–9.
33. Abe T, Mizobuchi Y, Sako W, Irahara S, Otomi Y, Obama Y, Nakajima K, Khashbat D, Majigsuren M, Kageji T, Nagahiro S, Harada M. Clinical Significance of Discrepancy between Arterial Spin La-

beling Images and Contrast-enhanced Images in the Diagnosis of Brain Tumors. Magn Reson Med Sci. 2015;14:313–9.
34. Wong AM, Yan FX, Liu HL. Comparison of Three-Dimensional Pseudo-continuous Arterial Spin Labeling Perfusion Imaging With Gradient-Echo and Spin-Echo Dynamic Susceptibility Contrast MRI. J Magn Reson Imaging. 2014;39:427–33.
35. Steketee RM, Mutsaerts HJ, Bron EE, van Osch MJ, Majoie CB, van der Lugt A, Nederveen AJ, Smits M. Quantitative Functional Arterial Spin Labeling (fASL) MRI – Sensitivity and Reproducibility of Regional CBF Changes Using Pseudo-Continuous ASL Product Sequences. PLoS One. 201514;10:e0132929.
36. Thomas AJ, Wiggins RH 3rd, Gurgel RK. Nonparaganglioma jugular foramen tumors. Otolaryngol Clin North Am. 2015;48:343–59.
37. Moreno-García C, González-García R, García MA, Monje F. Vagus Nerve Paraganglioma: Radiological Features We Should Be Aware of. J Maxillofac Oral Surg. 2015;14:1013–5.
38. He W, Chen F, Dalm B, Kirby PA, Greenlee JD. Metastatic involvement of the pituitary gland: a systematic review with pooled individual patient data analysis. Pituitary. 2015;18:159–68.
39. Hong P, Taylor SM, Trites JR, Bullock M, Nasser JG, Hart RD. Chondrosarcoma of the head and neck: report of 11 cases and literature review. J Otolaryngol Head Neck Surg. 2009;38:279–85.
40. Thomsen HS, Morcos SK, Almén T, Bellin MF, Bertolotto M, Bongartz G, Clement O, Leander P, Heinz-Peer G, Reimer P, Stacul F, van der Molen A, Webb JA; ESUR Contrast Medium Safety Committee. Nephrogenic systemic fibrosis and gadolinium-based contrast media: updated ESUR Contrast Medium Safety Committe guidelines. Eur Radiol. 2013;23:307–18.
41. Petcharunpaisan S, Ramalho J, Castillo M. Arterial Spin Labeling in neuroimaging. World J Radiol. 2010;2:384–98.
42. Mutsaerts HJ, van Osch MJ, Zelaya FO, Wang DJ, Nordhøy W, Wang Y, Wastling S, Fernandez-Seara MA, Petersen ET, Pizzini FB, Fallatah S, Hendrikse J, Geier O, Günther M, Golay X, Nederveen AJ, Bjørnerud A, Groote IR. Multi-vendor reliability of arterial spin labeling perfusion MRI using a near-identical sequence: implications for multi-center studies. Neuroimage. 2015;113:143–52.
43. Chen Y, Wang DJ, Detre JA. Test-retest reliability of arterial spin labeling with common labeling strategies. J Magn Reson Imaging. 2011;33:940–9.
44. Jung BC, Arevalo-Perez J, Lyo JK, Holodny AI, Karimi S, Young RJ, Peck KK. Comparison of Glioblastomas and Brain Metastases using Dynamic Contrast-Enhanced Perfusion MRI. J Neuroimaging. 2016;26:240–6.